Volume 1 | Number 1 | Jan 2013 | Pages 1–100

Nanoscale

www.rsc.org/nanoscale

ROYAL SOCIETY
OF CHEMISTRY

This is an *Accepted Manuscript*, which has been through the Royal Society of Chemistry peer review process and has been accepted for publication.

Accepted Manuscripts are published online shortly after acceptance, before technical editing, formatting and proof reading. Using this free service, authors can make their results available to the community, in citable form, before we publish the edited article. We will replace this *Accepted Manuscript* with the edited and formatted *Advance Article* as soon as it is available.

You can find more information about *Accepted Manuscripts* in the **Information for Authors**.

Please note that technical editing may introduce minor changes to the text and/or graphics, which may alter content. The journal's standard **Terms & Conditions** and the **Ethical guidelines** still apply. In no event shall the Royal Society of Chemistry be held responsible for any errors or omissions in this *Accepted Manuscript* or any consequences arising from the use of any information it contains.

www.rsc.org/nanoscale

Journal Name

Dynamic Article Links ▶

ARTICLE TYPE

Peptide-mediated Synthesis of Gold Nanoparticles: Effects of Peptide Sequence and Nature of Binding on Physicochemical Properties

Yue Li, *[1,#]* **Zhenghua Tang,** *[2,#]* **Paras N. Prasad,** *[3,4]* **Marc R. Knecht,** *[2,]* * **and Mark T. Swihart** *[1,]* *

Biomimetic nanotechnologies that use peptides to guide the growth and assembly of nanostructures offer new avenues for the creation of functional nanomaterials and manipulation of their physicochemical properties. However, the impacts of peptide sequence and binding motif upon the surface characteristics and physicochemical properties of nanoparticles remain poorly understood. The configurations of the biomolecules are expected to be extremely important for directing the synthesis and achieving desired material functionality, and
10 these binding motifs will vary with the peptide sequence. Here, we have prepared a series of Au nanoparticles capped with a variety of materials-directing peptides with known affinity for metal surfaces. These nanomaterials were characterized by UV-vis and circular dichroism spectroscopies, transmission electron microscopy, and ζ-potential measurement. Then their catalytic activity for 4-nitrophenol reduction was analyzed. The results indicate that substantially different Au/peptide interfaces are generated using different peptide sequences, even when these sequences have similar binding affinity. This is consistent with recent work showing that Au-peptide binding
15 affinity can have varying entropic and enthalpic contributions, with enthalpically- and entropically-driven binders exhibiting quite different ensembles of configurations on the Au surface. The catalytic activity, as reflected by the measured activation energy, did not correlate with the particle size or with the binding affinity of the peptides, suggesting that the reactivity of these materials is governed by the more subtle details of the conformation of the bound peptide and on the nanoparticle surface reconstruction as dictated by the peptide structure. Such variations in both nanoparticle surface reconstruction and peptide configuration could potentially be used to program
20 specific functionality into the peptide-capped nanomaterials.

Introduction

Peptide-based nanomaterial synthesis can provide new routes to functional inorganic/organic hybrid nanostructures that are prepared under sustainable biological conditions.[1-2] Furthermore,
25 the binding selectivity that can be achieved by using peptides opens the door to new applications, including bionanocombinatorics, defined as the controlled assembly of nanomaterials using biomolecular interactions.[3] Numerous studies have employed biological selection techniques, such as
30 phage display, to isolate Au-binding peptides;[4-5] however, a unifying theory to interpret and predict their surface binding affinities is only now emerging.[3] This analysis explicitly considers contributions of both enthalpic and entropic effects to the surface binding abilities of the peptides. The ensemble of
35 peptide structures on planar Au surfaces, as obtained from large-scale molecular simulation studies, revealed different structural motifs for peptides with comparable binding affinities.[3] When such peptides are used to cap Au nanoparticles, these structural differences are likely to translate to differences in other
40 physicochemical properties; however, no complete comparison of such biotic/abiotic effects for 3D Au nanomaterials has been presented. These effects have the potential to radically alter the nanoparticles' physicochemical properties and therefore their potential use in various applications. Comparative studies are
45 required to elucidate these effects.

Au nanomaterials have been heavily studied, mainly due to their versatile applications in catalysis,[6-7] energy capture and storage,[8-10] plasmonic sensors,[11] diagnostic tools,[12] and as components in complex nanoassemblies.[13-15] The optical
50 properties that arise from their localized surface plasmon resonance (LSPR) are sensitive to the size, shape, and aggregation state of the nanostructures. Catalytic applications of Au nanomaterials have also been intensely studied.[16-17] Such structures are known to be highly reactive for CO oxidation, but
55 only for sufficiently small Au particles, typically dispersed on a metal oxide support.[18-21] Only recently have the LSPR properties of such materials been observed to play a role in catalytic activity.[22-23] While these materials have demonstrated remarkable functionality in chemical transformations, the effects of the
60 ligands present on the particle surface remain unclear. For instance, thiols,[24-25] dendrimers,[26-27] and biomolecules[1, 7] have been used to generate catalytic Au materials; however, effects of ligand surface structure on the catalytic functionality remain poorly understood.

65 In this contribution, we correlate the peptide sequence, binding strength (including entropic and enthalpic contributions to binding), binding specificity, and surface-bound conformation to the size distribution, structure, and catalytic activity of Au nanoparticles capped with materials-directing peptides. We have
70 specifically focused on peptide-capped Au nanoparticles due to their great application potential, as well as the availability of recent studies that have isolated surface binding structures and thermodynamic parameters for a library of sequences under the

same conditions.[3] Here, these peptides have been used for the fabrication of aqueous dispersions of Au nanoparticles, providing a direct synthetic route for the generation of peptide-capped Au nanoparticles that is effective for many different sequences. The particles were fully characterized via UV-vis and circular dichroism (CD) spectroscopies, transmission electron microscopy (TEM), and ζ–potential analysis. Once fully characterized, their catalytic activity for the reduction of 4-nitrophenol to 4-aminophenol was analyzed as a model catalytic reaction.[28-29] The catalytic activity was found to depend upon the peptide binding to the particle surface. To this end, the surface-bound peptide can directly influence the interaction of reactants with the nanoparticle surface (steric effects on catalysis) and can also influence the surface reconstruction and electronic structure of the catalytic nanoparticle. From previous computational modeling,[3] the surface structures are expected to differ significantly between peptides based upon entropic and enthalpic considerations of surface binding. Several other studies have also used molecular simulation to investigate the nature of the gold-peptide interface.[30-31] These help to inform our understanding of this interface and also support the view that different sequences can be expected to have different surface structures. However, published simulation studies have been performed with different interaction potentials, sets of peptide sequences, simulation methodologies, and conditions. Thus, for our interpretation of the results we have relied primarily upon the recent simulation results of Tang et al.,[3] where all of the peptides used here were studied using the same methodology, potential, and conditions. As a result, the nature of the biotic/abiotic interface could substantially affect the physicochemical properties, including catalytic activities, of the Au materials.

Table 1. Sequences used for the generation of peptide-capped Au nanoparticles and properties of the final materials.

Peptide	Sequence	pI	ΔG (kJ/mol)	ζ-potential (mV)	Particle Size (nm)	Activation Energy (kJ/mol)
A3	AYSSGAPPMPPF	5.57	-31.8 ± 0.3	-27.6 ± 2.2	2.3 ± 0.5	20.0 ± 1.0
AgBP1	TGIFKSARAMRN	12.01	-31.6 ± 0.2	31.7 ± 0.4	3.2 ± 0.7	25.8 ± 3.1
AgBP2	EQLGVRKELRGV	8.85	-35.3 ± 1.2	34.5 ± 2.0	3.6 ± 1.0	15.1 ± 3.8
AuBP1	WAGAKRLVLRRE	11.71	-37.6 ± 0.9	32.2 ± 1.1	4.2 ± 1.1	NA
AuBP2	WALRRSIRRQSY	12	-36.4 ± 0.3	46.8 ± 8.0	3.8 ± 0.8	21.8 ± 1.2
GBP1	MHGKTQATSGTIQS	8.52	-37.6 ± 1.0	8.60 ± 1.6	3.2 ± 0.8	13.2 ± 0.4
Midas2	TGTSVLIATPYV	5.18	-35.7 ±1.2	-14.3 ± 2.6	5.1 ± 1.6	11.1 ± 0.5
Pd4	TSNAVHPTLRHL	9.47	-30.3 ± 0.2	30.6 ± 1.0	4.3 ± 1.7	13.6 ± 0.7
Z1	KHKHWHW	10	-31.3 ± 0.1	12.4 ± 3.2	3.9 ± 0.9	NA
Z2	RMRMKMK	12.02	-35.0 ± 0.6	36.0 ± 1.9	4.9 ± 1.5	9.1 ± 0.1

Experimental

Chemicals

Hydrogen tetrachloroaurate (HAuCl₄) was purchased from Acros Organics, while sodium borohydride (NaBH₄) was acquired from Sigma-Aldrich. 4-Nitrophenol, trifluoroacetic acid (TFA), and tri-isopropyl silane (TIS) were purchased from Alfa Aesar. All FMOC-protected amino acids, Wang resins, and peptide synthesis reagents (piperidine, *N,N'*-diisopropylethylamine (DIPEA), O-(benzotriazol-1-yl)-*N,N,N',N'*-tetramethyluronium hexafluorophosphate (HBTU), and *N*-hydroxybenzotriazole monohydrate (HOBt hydrate) were acquired from Advanced ChemTech. Ammonium hydroxide (20.0%), hydrogen peroxide

(30.0%), acetonitrile, methanol, and *N,N*-dimethylformamide were purchased from VWR. All of the chemicals were used as received. Finally, nanopure water (18.2 MΩ·cm; Millipore) was employed for all experiments.

Peptide Synthesis

All peptides were synthesized on a TETRAS model synthesizer (Creosalus), following standard solid-phase FMOC protocols.[32] Prior to purification, a cleavage cocktail with 95% TFA, 2.5% TIS, and 2.5% water was employed to cleave the peptides from the resin. The crude peptides were then purified via reverse phase HPLC and their sequences were confirmed by MALDI-TOF mass spectrometry.

Characterization

TEM analysis was conducted using a JEOL JEM-2010 microscope operating at a working voltage of 200 kV. The specimens were prepared by drop-casting 30 μL of the sample dispersion onto a carbon-coated 400 mesh Cu grid, which was allowed to dry under ambient environment. UV-vis optical absorbance of the Au nanoparticles was measured using a Shimadzu 3600 UV-visible-NIR scanning spectrophotometer employing a 1 cm quartz cuvette. CD spectra were measured using a Jasco J-815 CD spectrometer with a 1 cm quartz cuvette. All free peptides were diluted to a concentration of 8 μM and diluted nanoparticle dispersions with identical peptide contents were likewise prepared. The CDPro software package was used for secondary structure analysis.

Fabrication of Au Nanoparticles

To synthesize the peptide-capped nanoparticles, a previously developed protocol was adopted and refined.[33] Here, we describe a typical synthesis of AuBP1-capped Au nanoparticles with a Au: peptide ratio of 2. For this, 500 μL of a 1.0 mM aqueous solution of the AuBP1 peptide was first diluted in 4.460 mL of water in a vial. To this solution, 10 μL of 0.10 M HAuCl₄ in water was added. The pale yellow solution was vigorously stirred for at least 10 min, followed by the addition of 30 μL of a freshly prepared 0.10 M aqueous NaBH₄ solution. The resulting NaBH₄:Au ratio of 3 was found to be effective for generating colloidally stable materials. The reduction process produced an immediate color change from pale yellow to pink/red. The solution was further mixed using a vortex mixer, after which the reaction was allowed to proceed for 1.0 h at room temperature, without stirring, to ensure complete reduction. Identical methods were employed to produce Au nanoparticles capped with each of the peptides listed in Table 1 at a Au:peptide ratio of 2 for all syntheses.

Au Nanoparticle Catalyzed Reactions

The catalytic reduction of 4-nitrophenol to 4-aminophenol was conducted following previously described procedures.[29] Briefly, 1.0 mL of the as-prepared Au nanomaterial was added to 1.0 mL of a freshly prepared, aqueous NaBH₄ solution (15 mM) in a 3.5 mL quartz cuvette. The cuvette was then left undisturbed for 3.5 min. Next, 1.0 mL of a 150 μM 4-nitrophenol solution was added to the mixture to initiate the reaction. Under these conditions, the NaBH₄ is in significant excess, resulting in pseudo-first order kinetics with respect to the 4-nitrophenol substrate.[29] The reaction was monitored via time-resolved UV-vis analysis using an

Agilent 8453 spectrometer by recording spectra at 20.0 s intervals for 12.0 min at temperatures of 20 – 50 °C. Triplicate analyses were performed for every peptide-capped Au nanoparticle at each temperature.

Results and discussion

The ten peptides listed in **Table 1** were used to mediate Au nanoparticle growth via binding directly to the metallic surface. This set includes the following peptides: A3,[34] AuBP1,[35] AuBP2,[35] GBP1,[36] Midas2,[37] Z1,[38] and Z2,[38] known for Au binding, two Ag binding peptides, AgBP1[39,40] and AgBP2,[39,40] and a Pd binding peptide, Pd4.[33] The binding affinities (ΔG) of these peptide sequences on Au were recently quantified in experimental binding measurements using QCM, and are listed in Table 1.[3]

For the synthesis of peptide-capped Au nanoparticles, Au^{3+} ions were reduced in water using 3.0 equivalents of $NaBH_4$ in the presence of the selected biomolecules. For all of the systems, a Au:peptide molar ratio of 2 was employed and no bulk material precipitation was observed for any of the reactions under these conditions. This indicated that the biomolecules capped the nanoparticles to limit their growth and prevent aggregation. The generated particles remained dispersed in solution with no obvious changes for at least 1 week, demonstrating the colloidal sta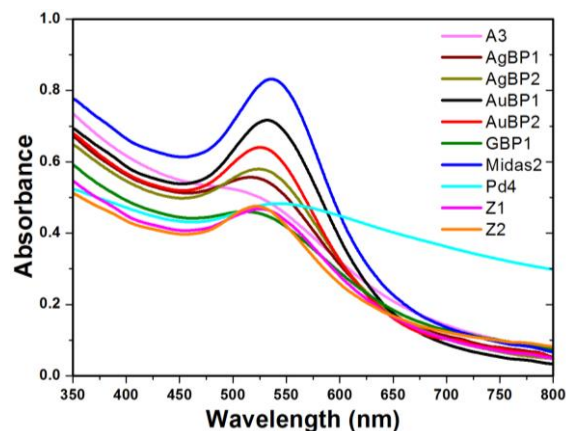bility of the peptide-capped materials. Long-term stability varied, with some samples remaining stable after a few months. Pd4-capped particles were the least stable, typically beginning to show signs of aggregation after about 1 week. For Au:peptide ratios greater than 2, aggregation and precipitation were observed for most of the peptides, thus only one ratio was studied to allow for direct comparison of the results between peptides. The effect of increasing the Au:peptide ratio on particle size and shape is illustrated for one peptide, AuBP1, in the supporting information (Fig. S1). Interestingly, an additional Au binding-peptide, B1,[41-42] with a binding affinity (ΔG) value of -36.6 ± 1.2 kJ/mol for a polycrystalline Au target surface,[3] was employed to generate Au nanoparticles under the same conditions; however, unstable materials that rapidly precipitated were produced. This suggests that additional binding parameters beyond simple surface affinity may govern particle formation using biomolecules.

Once stable materials were generated, the particles were examined via a variety of techniques. Initially, UV-vis spectroscopy, as shown in Fig. 1, was used to analyze the optical properties. An LSPR absorbance peak at or near 520 nm was observed in almost all cases, consistent with formation of Au

Fig. 1. UV-vis extinction spectra of the peptide-capped Au nanoparticles prepared using the indicated sequences.

nanoparticles larger than 2 nm in diameter. However, notable deviations from this behavior were also observed. For the Pd4 peptide, a weak Au-binder that was originally isolated for Pd-binding affinity,[33] the UV-vis spectrum displays a broad absorbance that extends to longer wavelengths. This could arise from either aggregation of smaller particles to form larger structures or from the formation of a polydisperse population of particles. Additionally, particles capped with the Z1 peptide displayed an absorbance shoulder over a strong plasmon band at 520 nm. This also suggests that a greater degree of polydispersity or aggregation in solution for this material than for the other samples. Absorption at a shorter wavelength and a less pronounced plasmon resonance is often associated with a smaller particle size (near or below 2 nm), but this was not reflected in the size distributions from TEM imaging of this sample (Fig. 2, Fig. S2).

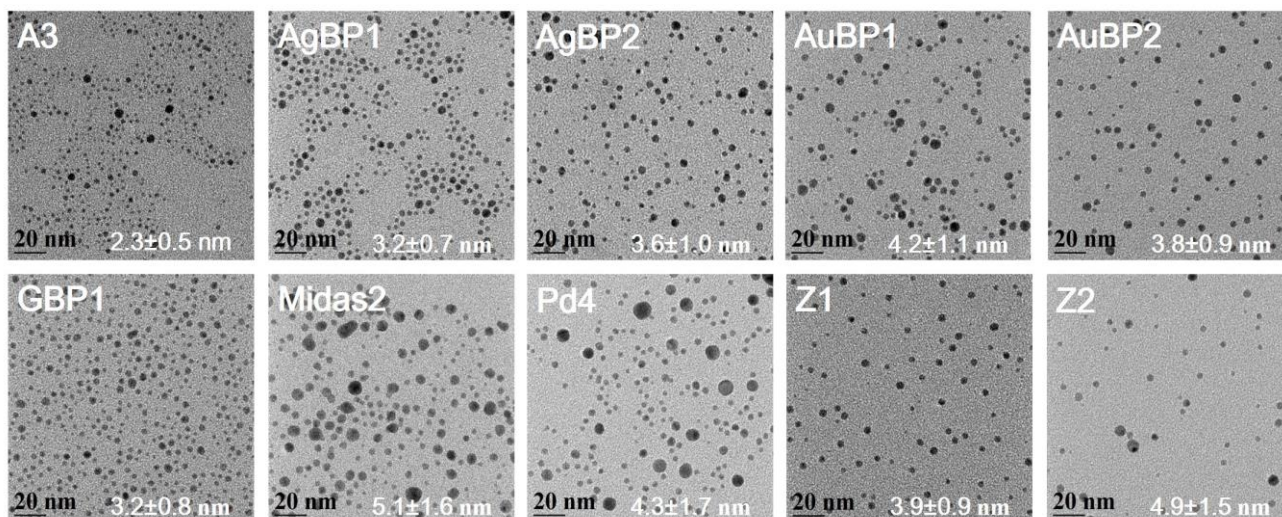TEM analysis was used to obtain more direct information

Fig 2. TEM analysis of the peptide-capped Au nanoparticles prepared using the indicated sequences.

about particle size and shape. Fig. 2 presents TEM images of the Au nanoparticles prepared using the selected peptides, while Table 1 displays the particle sizes of materials obtained using each peptide. These values are presented as an average of at least 100 nanoparticles ± one standard deviation. Complete size distribution histograms are available in the Supporting Information (Fig. S2). In general, the size of the peptide-capped Au nanoparticles varied over a relatively small range from 2.3 ± 0.5 nm for the structures prepared using the A3 sequence to 5.1 ± 1.6 nm for the Midas2-capped particles. Furthermore, all of the particles were spherical in shape and have a fairly narrow size distribution for materials in this size regime. All of the particles presented here were prepared at a Au:peptide ratio of 2. For reactions carried out at higher ratios, larger nanoparticles of irregular shapes were often observed. These were generally colloidally unstable and precipitated out of solution. The Pd4-capped sample that displayed a broad UV-vis absorbance was also one of the most polydisperse in size, with a bimodal particle population. Furthermore, no clear trend was evident between the previously reported binding strengths of the peptides[3] and the size of the particles produced (Table 1). For example, the AuBP1 and GBP1 peptides have the strongest affinity for Au based upon ΔG values; however, these sequences generated Au nanoparticles with average diameters of 4.2 ± 1.1 and 3.2 ± 0.8 nm, respectively, which were neither the largest or smallest among the various peptides examined. The particles fabricated with the Pd4-peptide, which has the lowest affinity for Au among these peptides, had a mean diameter of 4.3 ± 1.7 nm, almost identical to the diameter for AuBP1. This suggests that other factors beyond simple binding affinity play an important role in governing interactions between peptides and growing nanoparticles. These may include the specific amino acids that coordinate to the surface in each case, the spacing between them, and their electrostatic charge under synthesis conditions, as well as other factors affecting biorecognition. Further characterization of the particles using ζ-potential analysis (Table 1) demonstrated an increased surface potential with increasing pI value of the peptide, as would be expected if the charge state of the bound peptide is the same as in solution. The two peptides with a pI <7 produced particles with negative ζ-potentials, while all of the others generated materials with a positive ζ-potential.

CD spectroscopy was performed to explore the structural change of the peptides upon binding to the Au nanoparticle surfaces. Collectively, the CD spectra (Supporting Information, Fig. S3) revealed that most peptides became less structured when bound to the material, as indicated by a decrease in ellipticity. The secondary structure analysis obtained using CDPro software indicated that both free and nanoparticle-bound peptides contain a large fraction of unordered structure (42%~48%), as is to be expected for these relatively short sequences. The decreased ellipticity of bound peptides suggests that contact with the Au surface during the synthesis somewhat altered the secondary structure of the peptides to accommodate the Au nanoparticle. This is most evident for the strong binding peptides whose binding affinities are enthalpically driven by their anchor residues (AuBP1, AuBP2, etc.).[3] Note that enthalpically-driven surface binding peptides anchor to the Au interface at multiple residues dispersed through the entire sequence. In contrast, some peptides
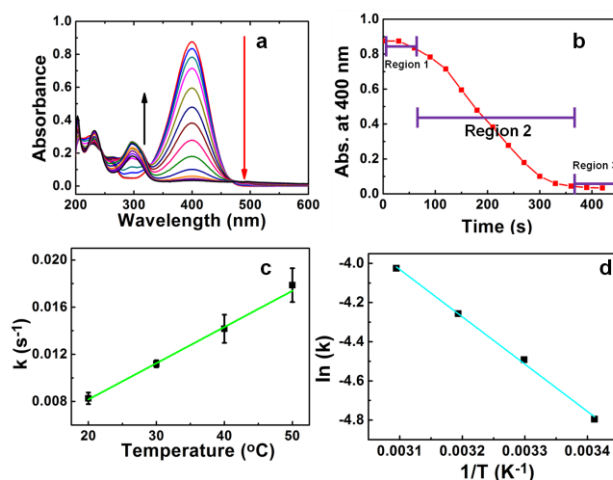

Fig. 3. Kinetic analysis of catalytic reduction of 4-nitrophenol using A3 peptide-capped nanoparticles: (a) UV-vis spectra during the course of the reaction; (b) absorbance at 400 nm as a function of time; (c) pseudo first order rate constant vs. temperature; and (d) Arrhenius plot from which the activation energy was calculated.

only show a slight ellipticity change or even no evident change. This is likely an effect of those peptides having fewer contact residues with strong binding affinities and relatively high conformational entropy contributions, where a large fraction of the biomolecule remains unbound on the Au surface, thus giving rise to a modest structural change between bound and unbound states. This is especially true in the case of GBP1; it can mediate the synthesis of relatively small nanoparticles but shows minimal change in ellipticity (Fig. S1h).

Once the peptide-capped Au nanoparticles were fully characterized, their catalytic activity was analyzed and compared using the reduction of 4-nitrophenol to 4-aminophenol as a probe reaction. This reaction occurs directly on the particle surface following a Langmuir-Hinshelwood mechanism.[29, 43] Thus, changes induced by the peptide structure are likely to be reflected in changes in catalytic activity, *i.e.* reaction rate and activation energy. The reaction was carried out using a large excess of $NaBH_4$, such that its concentration remained essentially constant during the experiments. As such, pseudo first order reaction kinetics can be assumed with respect to the 4-nitrophenol substrate.[44] The reaction kinetics were monitored through time-resolved UV-vis spectroscopy. The substrate has a strong characteristic absorption at 400 nm, while the product, 4-aminophenol, absorbs at ~310 nm. A typical UV-vis analysis of the system as a function of time is presented in Fig. 3a for the reaction catalyzed using the A3 peptide-capped Au nanoparticles at 20 °C. Here, a gradual decrease in the 400 nm absorption peak was observed, in conjunction with an increase at 310 nm, both of which reflect reaction progression. Additionally, it is worth noting that an isosbestic point was not observed in the analysis, agreeing with previous reports.[37-38] This effect was attributed to the scattering caused by H_2 generation during the reduction process by $NaBH_4$. Similar results were observed at higher temperatures, albeit with faster reaction kinetics. Triplicate analyses were conducted for each Au nanoparticle catalyst over the selected temperature range, and all of the materials were
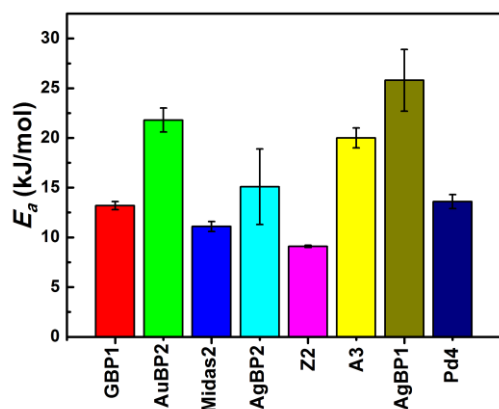
Fig. 4. Comparison of the E_a values for the different peptide-capped Au nanoparticle catalysts. Note that values for the AuBP1- and Z1-capped materials are not presented as these structures are not stable at high temperatures, thus the activation energies were not computed.

tested under identical reaction conditions.

For this system, the reaction rate constant can be determined through the change in the 400 nm absorbance.[43, 45] As shown in Fig. 3b, three discrete reaction stages can be identified from this
5 change: an induction period (0-50 s), a reaction period (50-350 s), and a completion period (>350 s). In the induction period, the absorbance remained nearly constant. During this time, adsorption of 4-nitrophenol on the metallic surface occurs, possibly accompanied by other surface rearrangements. At the
10 end of the induction period, the surface is catalytically active and the reaction can proceed, as evidenced by the change in absorbance noted in the second region. Once the reaction is complete, no change in the absorption is again noted (region 3). From region 2 where the actual reaction is progressing, the rate
15 constant (k) can be determined using pseudo first order kinetic fitting of the data, as in many previous reports using this reaction as a probe of catalytic activity.[28, 46-47] As shown in Fig. 3c, the reaction rate constants of the A3-capped Au nanoparticles ranged from 0.0083 ± 0.0005 to 0.0179 ± 0.0014 s^{-1} at 20 °C and 50 °C,
20 respectively. To obtain the activation energy (E_a) for the reaction catalyzed with each peptide-capped nanoparticle, the natural log of the reaction rate constants were plotted as a function of inverse temperature (an Arrhenius plot). The slope of the best-fit line of the data is $-E_a/R$ (Fig. 3d). From this analysis, the activation
25 energy for the reaction catalyzed by the A3-capped Au nanoparticles was 20.0 ± 1.0 kJ/mol.

Results of this analysis for all of the peptide-capped Au nanoparticles of the study are summarized in Table 1 and Fig. 4. For AuBP1 and Z1, at higher temperatures, the particles
30 aggregated and precipitated. Thus, E_a values could not be obtained for particles capped with these sequences. For the other materials analyzed, the activation energies ranged from 9.05 ± 0.1 kJ/mol for the Z2-capped particles to 25.6 ± 3.1 kJ/mol for the structures passivated with the AgBP1 peptide. Overall, these
35 activation energies are smaller than those observed for Au nanoparticle networks templated by the R5 peptide (27.7 - 29.0 kJ/mol).[28] In that case, the R5 peptide forms a 3D scaffold in solution, within which metallic nanostructures are encapsulated,

in the form of linear, branching nanoparticle networks. Thus,
40 these materials should not be directly compared with the present peptide-capped spherical Au nanoparticles.

Once the E_a values were determined for all of the different peptide-capped Au nanoparticles, the results were analyzed for any trends with respect to particle size or binding affinity of the
45 peptides. For this, the activation energies were compared with the particle size and ΔG values for peptide/Au binding; however, no trends in the reactivity were apparent, as shown in the Supporting Information (Fig. S4). Thus, the variations in catalytic activity can likely be attributed to the structural details of the Au/peptide
50 interface developed at the nanoparticle surface.

The catalytic activity can also be viewed in light of recent molecular dynamics studies of binding of these peptides on atomically flat Au surfaces.[3] There, the enthalpic and entropic contributions to binding were analyzed. Each peptide was
55 classified as having "strong", "medium", or "weak" anchors, based on the number of strongly binding residues. These anchor residues determine the binding enthalpy. Each peptide was also classified as having "high", "medium", or "low" conformational entropy, based on the number of biomolecular conformations
60 possible for the bound peptide. Sequences with many anchors distributed throughout the peptide tend to have low entropy scores. Comparing the activation energies measured here with those classifications shows that the nanocrystals with the three highest average activation energies, >20 kJ/mol, were all
65 classified as having "strong" anchors, thus being enthalpically driven binding peptides. The two nanocrystal samples that precipitated at elevated temperature, and for which E_a values were not available, were also coated with peptides classified as having "strong" anchors. The remaining nanoparticles, with
70 average activation energies from 9.1 to 15.1 kJ/mol were coated with peptides classified as having "medium" or "weak" anchors. Thus, based upon this limited set of sequences, we tentatively suggest that the presence of a relatively large number of strongly-binding residues dispersed throughout the sequence decreases the
75 catalytic activity. At least for this set of peptides, this anchor score shows much greater correlation with the measured activation energies than does the overall binding affinity, the particle size, or the conformational entropy score. The peptides that exhibit enthalpically-driven binding tend to lay flat on the Au
80 surface, thus diminishing the amount of reactive metal surface area available for catalytic activity. This results in the observed changes in the reaction rates and activation energies. Taken together, these observations provide new information that can be used for the design of biomolecular ligands that maximize
85 catalytic activity while binding strongly to the surface and providing colloidal stability. In this regard, nanocatalysts capped with ligands that possess limited anchor points and extend from the surface may have increased catalytic activity. This assumes that limited inter-ligand interactions are present, as these
90 interactions could inhibit substrate diffusion to the active metal surface. These results should also be applicable to other non-biological catalytic systems; however, additional research is required to demonstrate that.

The peptide-Au interface can play multiple roles in controlling
95 the reactivity, through steric and/or electronic effects. Steric considerations likely play a dominant role in the reactivity by

limiting access of the bulky 4-nitrophenol reagent to the catalytic
surface, thus lowering the reactivity, particularly for peptides that
feature multiple strong anchoring residues. Clearly, changes in
binding motif and variations in the surface structure and steric
5 effects upon varying the peptide sequence produce the varied E_a
values. Additionally, changes to the particle surface
reconstruction and electronic structure based upon the peptide
sequence are likely. Computational studies have shown
significant mixing of orbitals in metallic cluster or nanoparticles
10 with those of ligands, even for relatively weakly-interacting
lgands.[48-49] This may also play a role in the chemical reactivity.
Further experimental and computational studies are underway, to
explore the nature of these nanoparticle interfaces in greater detail.

Conclusions

15 In summary, the synthesis, characterization, and catalytic
performance of Au nanoparticles capped with ten different
materials binding peptides were demonstrated. These
nanomaterials were generated via a simple reduction approach,
which provides a general synthetic route that produced particles
20 of similar size using many different peptides of varied binding
affinity. The resulting Au nanoparticles were generally spherical
with a relatively narrow size distribution. All of the peptide-
capped Au nanoparticles demonstrated catalytic activity for the
reduction of 4-nitrophenol. The rate constants at different
25 temperatures were measured, from which the activation energies
for this reaction were determined and compared. From this, the
catalytic activity, as reflected by the E_a values, and the absolute
reaction rates, did not correlate simply with the particle size or
with the known binding affinity of the peptides on Au surfaces.
30 This suggests that the reactivity of these materials is governed by
the more subtle details of the conformation of the bound peptide
and on the reconstructed nanoparticle surface as dictated by the
peptide structure. These results demonstrate unique biomolecular
surface effects that are important for the use of peptides in the
35 development of functional nanoparticles that exploit surface-
based activities.

Acknowledgements

40 **Notes**

[1] *Department of Chemical and Biological Engineering, University at
Buffalo (SUNY), Buffalo, NY 14260, Email: swihart@buffalo.edu*
[2] *Department of Chemistry, University of Miami. 1301 Memorial Drive,
Coral Gables, Florida 33146, Email: knecht@miami.edu*
45 [3] *Department of Chemistry and Institute for Laser Photonics and
Biophotonics, University at Buffalo (SUNY), Buffalo, NY 14260*
[4] *Department of Chemistry, Korea University, Seoul, Korea*
#: These authors contributed equally.
† Electronic Supplementary Information (ESI) available: Size
50 distributions from TEM analysis, CD spectra of free and nanoparticle-
bound peptides, and relationships between activation energy, particle size,
and binding affinity. See DOI: 10.1039/b000000x/

References

55 1. Briggs, B. D.; Knecht, M. R., Nanotechnology Meets Biology:
Peptide-based Methods for the Fabrication of Functional Materials. *J.
Phys. Chem. Lett.* **2012,** *3*, 405-418.

2. Sarikaya, M.; Tamerler, C.; Jen, A. K. Y.; Schulten, K.; Baneyx, F.,
Molecular Biomimetics: Nanotechnology Through Biology. *Nat. Mater.*
60 **2003,** *2*, 577-585.

3. Tang, Z.; Palafox-Hernandez, J. P.; Law, W.-C.; E. Hughes, Z.;
Swihart, M. T.; Prasad, P. N.; Knecht, M. R.; Walsh, T. R., Biomolecular
Recognition Principles for Bionanocombinatorics: An Integrated
Approach To Elucidate Enthalpic and Entropic Factors. *ACS Nano* **2013,**
65 *7*, 9632-9646.

4. Naik, R. R.; Jones, S. E.; Murray, C. J.; McAuliffe, J. C.; Vaia, R. A.;
Stone, M. O., Peptide Templates for Nanoparticle Synthesis Derived
From Polymerase Chain Reaction-Driven Phage Display. *Adv. Func.
Mater.* **2004,** *14*, 25-30.

70 5. Hoess, R. H., Protein Design and Phage Display. *Chem. Rev.* **2001,**
101, 3205-3218.

6. Coppage, R.; Slocik, J. M.; Sethi, M.; Pacardo, D. B.; Naik, R. R.;
Knecht, M. R., Elucidation of Peptide Effects that Control the Activity of
Nanoparticles. *Angew. Chem. Int. Ed.* **2010,** *49*, 3767-3770.

75 7. Bhandari, R.; Coppage, R.; Knecht, M. R., Mimicking Nature's
Strategies for the Design of Nanocatalysts. *Catal. Sci. Technol.* **2012,** *2*,
256-266.

8. Lee, Y. J.; Lee, Y.; Oh, D.; Chen, T.; Ceder, G.; Belcher, A. M.,
Biologically Activated Noble Metal Alloys at the Nanoscale: For Lithium
80 Ion Battery Anodes. *Nano Lett.* **2010,** *10*, 2433-2440.

9. Lee, Y.; Kim, J.; Yun, D. S.; Nam, Y. S.; Shao-Horn, Y.; Belcher, A.
M., Virus-Templated Au and Au-Pt Core-Shell Nanowires and Their
Electrocatalytic Activities for Fuel Cell Applications. *Energy Environ. Sci.*
2012, *5*, 8328-8334.

85 10. Halas, N. J., Plasmonics: An Emerging Field Fostered by Nano
Letters. *Nano Lett.* **2010,** *10*, 3816-3822.

11. Saha, K.; Agasti, S. S.; Kim, C.; Li, X. N.; Rotello, V. M., Gold
Nanoparticles in Chemical and Biological Sensing. *Chem. Rev.* **2012,** *112*,
2739-2779.

90 12. Rosi, N. L.; Mirkin, C. A., Nanostructures in Biodiagnostics. *Chem.
Rev.* **2005,** *105*, 1547-1562.

13. Kim, Y.; Macfarlane, R. J.; Mirkin, C. A., Dynamically
Interchangeable Nanoparticle Superlattices Through the Use of Nucleic
Acid-Based Allosteric Effectors. *J. Am. Chem. Soc.* **2013,** *135*, 10342-
95 10345.

14. Zhang, C.; Macfarlane, R. J.; Young, K. L.; Choi, C. H. J.; Hao, L.;
Auyeung, E.; Liu, G.; Zhou, X.; Mirkin, C. A., A General Approach to
DNA-Programmable Atom Equivalents. *Nat. Mater.* **2013,** *12*, 741-746.

15. Macfarlane, R. J.; Jones, M. R.; Lee, B.; Auyeung, E.; Mirkin, C. A.,
100 Topotactic Interconversion of Nanoparticle Superlattices. *Science* **2013,**
341, 1222-1225.

16. Grabow, L. C.; Mavrikakis, M., Nanocatalysis Beyond the Gold-
Rush Era. *Angew. Chem., Int. Ed.* **2008,** *47*, 7390-7392.

17. Chen, M.; Goodman, D. W., Catalytically Active Gold: From
105 Nanoparticles to Ultrathin Films. *Acc. Chem. Res.* **2006,** *39*, 739-746.

18. Gong, J.; Mullins, C. B., Surface Science Investigations of Oxidative
Chemistry on Gold. *Acc. Chem. Res.* **2009,** *42*, 1063-1073.

19. Long, C. G.; Gilbertson, J. D.; Vijayaraghavan, G.; Stevenson, K. J.;
Pursell, C. J.; Chandler, B. D., Kinetic Evaluation of Highly Active
110 Supported Gold Catalysts Prepared From Monolayer-Protected Clusters:

An Experimental Michaelis-Menten Approach for Determining the Oxygen Binding Constant During CO Oxidation Catalysis. *J. Am. Chem. Soc.* **2008**, *130*, 10103-10115.

20. Hartshorn, H.; Pursell, C. J.; Chandler, B. D., Adsorption of CO on Supported Gold Nanoparticle Catalysts: A Comparative Study. *J. Phys. Chem. C* **2009**, *113*, 10718-10725.

21. Laoufi, I.; Saint-Lager, M. C.; Lazzari, R.; Jupille, J.; Robach, O.; Garaudee, S.; Cabailh, G.; Dolle, P.; Cruguel, H.; Bailly, A., Size and Catalytic Activity of Supported Gold Nanoparticles: An in Operando Study during CO Oxidation. *J. Phys. Chem. C* **2011**, *115*, 4673-4679.

22. Hung, W. H.; Aykol, M.; Valley, D.; Hou, W.; Cronin, S. B., Plasmon Resonant Enhancement of Carbon Monoxide Catalysis. *Nano Lett.* **2010**, *10*, 1314-1318.

23. Liu, Z.; Hou, W.; Pavaskar, P.; Aykol, M.; Cronin, S. B., Plasmon Resonant Enhancement of Photocatalytic Water Splitting Under Visible Illumination. *Nano Lett.* **2011**, *11*, 1111-1116.

24. Zhu, Y.; Qian, H.; Drake, B. A.; Jin, R., Atomically Precise Au25(SR)(18) Nanoparticles as Catalysts for the Selective Hydrogenation of alpha,beta-Unsaturated Ketones and Aldehydes. *Angew. Chem., Int. Ed.* **2010**, *49*, 1295-1298.

25. Zhu, Y.; Qian, H.; Jin, R., Catalysis Opportunities of Atomically Precise Gold Nanoclusters. *J. Mater. Chem.* **2011**, *21*, 6793-6799.

26. Yancey, D. F.; Carino, E. V.; Crooks, R. M., Electrochemical Synthesis and Electrocatalytic Properties of Au@Pt Dendrimer-Encapsulated Nanoparticles. *J. Am. Chem. Soc.* **2010**, *132*, 10988-10989.

27. Lyyamperumal, R.; Zhang, L.; Henkelman, G.; Crooks, R. M., Efficient Electrocatalytic Oxidation of Formic Acid Using Au@Pt Dendrimer-Encapsulated Nanoparticles. *J. Am. Chem. Soc.* **2013**, *135*, 5521-5524.

28. Bhandari, R.; Knecht, M. R., Synthesis, Characterization, and Catalytic Application of Networked Au Nanostructures Fabricated using Peptide Templates. *Catal. Sci. Technol.* **2012**, *2*, 1360-1366.

29. Wunder, S.; Polzer, F.; Lu, Y.; Mei, Y.; Ballauff, M., Kinetic Analysis of Catalytic Reduction of 4-Nitrophenol by Metallic Nanoparticles Immobilized in Spherical Polyelectrolyte Brushes. *J. Phys. Chem. C* **2010**, *114*, 8814-8820.

30. Corni, S.; Hnilova, M.; Tamerler, C.; Sarikaya, M., Conformational Behavior of Genetically-Engineered Dodecapeptides as a Determinant of Binding Affinity for Gold. *J Phys Chem C* **2013**, *117*, 16990-17003.

31. Heinz, H.; Farmer, B. L.; Pandey, R. B.; Slocik, J. M.; Patnaik, S. S.; Pachter, R.; Naik, R. R., Nature of Molecular Interactions of Peptides with Gold, Palladium, and Pd-Au Bimetal Surfaces in Aqueous Solution. *J Am Chem Soc* **2009**, *131*, 9704-9714.

32. Chan, W. C.; White, P. D., *Fmoc Solid Phase Peptide Synthesis: A Practical Approach*. Oxford Univ. Press: New York, 2000.

33. Pacardo, D. B.; Sethi, M.; Jones, S. E.; Naik, R. R.; Knecht, M. R., Biomimetic Synthesis of Pd Nanocatalysts for the Stille Coupling Reaction. *ACS Nano* **2009**, *3*, 1288-1296.

34. Slocik, J. M.; Stone, M. O.; Naik, R. R., Synthesis of Gold Nanoparticles Using Multifunctional Peptides. *Small* **2005**, *1*, 1048-1052.

35. Hnilova, M.; Oren, E. E.; Seker, U. O. S.; Wilson, B. R.; Collino, S.; Evans, J. S.; Tamerler, C.; Sarikaya, M., Effect of Molecular Conformations on the Adsorption Behavior of Gold-Binding Peptides. *Langmuir* **2008**, *24*, 12440-12445.

36. Brown, S.; Sarikaya, M.; Johnson, E., A Genetic Analysis of Crystal Growth. *J. Mol. Biol.* **2000**, *299*, 725-735.

37. Kim, J.; Rheem, Y.; Yoo, B.; Chong, Y.; Bozhilov, K. N.; Kim, D.; Sadowsky, M. J.; Hur, H.-G.; Myung, N. V., Peptide-Mediated Shape- and Size-Tunable Synthesis of Gold Nanostructures. *Acta Biomateria* **2010**, *6*, 2681-2689.

38. Peelle, B. R.; Krauland, E. M.; Wittrup, K. D.; Belcher, A. M., Design Criteria for Engineering Inorganic Material-Specific Peptides. *Langmuir* **2005**, *21*, 6929-6933.

39. Hnilova, M.; Liu, X.; Yuca, E.; Jia, C.; Wilson, B.; Karatas, A. Y.; Gresswell, C.; Ohuchi, F.; Kitamura, K.; Tamerler, C., Multifunctional Protein-Enabled Patterning on Arrayed Ferroelectric Materials. *ACS Appl. Mater. Interfaces* **2012**, *4*, 1865-1871.

40. Sedlak, R. H.; Hnilova, M.; Grosh, C.; Fong, H.; Baneyx, F.; Schwartz, D.; Sarikaya, M.; Tamerler, C.; Traxler, B., Engineered Escherichia coli Silver-Binding Periplasmic Protein That Promotes Silver Tolerance. *Appli. Environ. Microbiol.* **2012**, *78*, 2289-2296.

41. Whaley, S. R.; English, D. S.; Hu, E. L.; Barbara, P. F.; Belcher, A. M., Selection of Peptides with Semiconductor Binding Specificity for Directed Nanocrystal Assembly. *Nature* **2000**, *405*, 665-668.

42. Nam, K. T.; Kim, D. W.; Yoo, P. J.; Chiang, C. Y.; Meethong, N.; Hammond, P. T.; Chiang, Y. M.; Belcher, A. M., Virus-Enabled Synthesis and Assembly of Nanowires for Lithium Ion Battery Electrodes. *Science* **2006**, *312*, 885-888.

43. Wunder, S.; Lu, Y.; Albrecht, M.; Ballauff, M., Catalytic Activity of Faceted Gold Nanoparticles Studied by a Model Reaction: Evidence for Substrate-Induced Surface Restructuring. *ACS Catal.* **2011**, *1*, 908-916.

44. Behrens, S.; Heyman, A.; Maul, R.; Essig, S.; Steigerwald, S.; Quintilla, A.; Wenzel, W.; Burck, J.; Dgany, O.; Shoseyov, O., Constrained Synthesis and Organization of Catalytically Active Metal Nanoparticles by Self-Assembled Protein Templates. *Adv. Mater.* **2009**, *21*, 3515-3519.

45. Zeng, J.; Zhang, Q.; Chen, J.; Xia, Y., A Comparison Study of the Catalytic Properties of Au-Based Nanocages, Nanoboxes, and Nanoparticles. *Nano Lett.* **2010**, *10*, 30-35.

46. Johnson, J. A.; Makis, J. J.; Marvin, K. A.; Rodenbusch, S. E.; Stevenson, K. J., Size-Dependent Hydrogenation of *p*-Nitrophenol with Pd Nanoparticles Synthesized with Poly(amido)amine Dendrimer Templates. *J. Phys. Chem. C* **2013**, *117*, 22644-22651.

47. Pozun, Z. D.; Rodenbusch, S. E.; Keller, E.; Tran, K.; Tang, W.; Stevenson, K. J.; Henkelman, G., A Systematic Investigation of *p*-Nitrophenol Reduction by Bimetallic Dendrimer Encapsulated Nanoparticles. *J. Phys. Chem. C* **2013**, *117*, 7598-7604.

48. Rinkevicius, Z.; Autschbach, J.; Baev, A.; Swihart, M.; Agren, H.; Prasad, P. N., Novel Pathways for Enhancing Nonlinearity of Organics Utilizing Metal Clusters. *J. Phys. Chem. A* **2010**, *114*, 7590-7594.

49. Morton, S. M.; Silverstein, D. W.; Jensen, L., Theoretical Studies of Plasmonics using Electronic Structure Methods. *Chem. Rev.* **2011**, *111*, 3962-3994.